4th URSI AT-RASC, Gran Canaria, 19 – 24 May 2024

Metalmesh-based Reconfigurable Intelligent Surface for Wi-Fi 6E Applications

S. I. Inácio and L. M. Pessoa*
INESC TEC and Faculdade de Engenharia, Universidade do Porto, Porto, Portugal

Abstract

This paper presents an optically transparent 2-bit unit-cell for reflective intelligent surface applications in Wi-Fi 6E. The unit-cell is based on a metalmesh and can be reconfigured electronically by adjusting the voltage applied to a varactor diode. The performance of the RIS is demonstrated through simulation, which shows that the results are in good agreement with the theoretical predictions.

1 Introduction

Numerous electronic devices today employ Wi-Fi technology for efficient connectivity. Wi-Fi 5 (802.11ac) and Wi-Fi 6 (802.11ax) are two commonly used Wi-Fi standards that operate on the frequency bands of 2.4 GHz and 5 GHz [1]. However, these frequency ranges may pose challenges for high-speed and low-latency internet connections in the future. To address this issue, a new Wi-Fi standard, known as Wi-Fi 6E (extended), has been developed to operate on a frequency range of 5.925 to 7.125 GHz. As a result, there has been an exploration of antennas suitable for Wi-Fi 6E to enhance the performance of this new standard [2, 3]. However, almost all of these antennas are not transparent to light or not reconfigurable, which may pose a design challenge, in aesthetic concerns, for smart homes and cities.

Transparent antennas are typically fabricated on a substrate made of glass or plastic, and they can be classified into two main categories: mesh antennas and thin-film antennas [4]. Mesh antennas are usually constructed using conventional opaque conductive materials like copper, gold, or silver, that have patterned holes to allow light to pass through. On the other hand, thin-film antennas attain their transparency from materials that possess both high optical transparency and electrical conductivity. Meshed conductors have a lower sheet resistance compared to thin films (conductive oxide or conductive polymer, for example), and so higher electrical conductivity. However, their optical transparency is also lower than these films [5]. On substrates that possess optical transparency, such as Polyethylene Glycol Terephthalate (PET), the metalmesh is barely visible as it is composed of ultrafine metal gridlines. The widths of these gridlines are typically less than 10 μm, while their spacings vary between 150 μm to 300 μm [5].

Reflective Intelligent Surfaces (RIS) are poised to play a pivotal role in shaping the future of smart radio environments. These surfaces can be strategically deployed in various settings, including building walls (and, if transparent, in windows) to enhance diverse aspects of wireless communication [6]. For example, they can provide uninterrupted connectivity, by dynamically adjusting their radiation characteristics, and improve the quality of service in uncontrolled environments, such as large cities, where wireless control is limited. Reconfigurability is a fundamental aspect of RIS, which is achieved by manipulating the electromagnetic response of its unit-cells. Various techniques can accomplish this. The most common method involves the utilization of active elements such as PIN diodes, varactors, and radiofrequency micro-electromechanical system switches [7].

The present work proposes a high optical transparency two-bit metalmesh-based RIS suitable for Wi-Fi 6E applications. The unit-cell consists of a metalmesh patch antenna loaded with a varactor diode to achieve reconfigurability by applying a bias voltage. The ground is implemented by metal stripes to further enhance the optical transparency.

2 Optically Transparent Unit-cell

2.1 Single Layer Optically Transparent Structures

Figure 1 shows a partial schematic of the two studied single-layer structures. Both structures employ polyethylene terephthalate (PET) substrates. The first structure consists of a square metal mesh having a mesh width (w) and a mesh spacing (s). This square configuration was chosen for its desirable properties such as high flexibility, compactness, lightweight, transparency, and mechanical robustness. The second structure considers only the vertical lines of the mesh. The electromagnetic shielding properties of both structures will be studied and compared under y-polarized waves incidence, to evaluate their potential use in the ground layer of the RIS unit-cell.

2.2 Optical and Electrical Properties

The optical transparency (OT) of a metalmesh, i.e. the percentage of light transmitted through it, is defined as the ra-

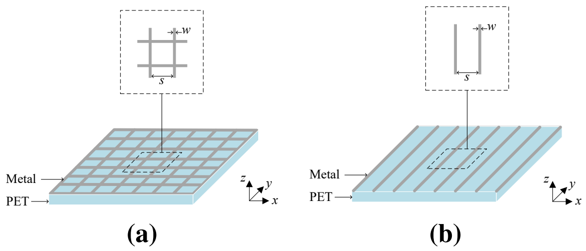

Figure 1. Structures: (a) metalmesh and (b) metal stripes.

tio between the open area and the total area [8]. So, the OT of a square with side length $(s+w)$ and open area $(s \times s)$, and therefore of the meshed metal layer represented on the structure of Figure 1 (a) is given by:

$$\mathrm{OT} = \left(\frac{s}{s+w}\right)^2. \tag{1}$$

In the case of the structure of Figure 1 (b), the OT is improved by eliminating the horizontal lines, calculated as:

$$\mathrm{OT} = \frac{s}{s+w}. \tag{2}$$

When metalmesh layers are employed on a substrate, as in the structures considered, it is necessary to take into account the optical reflectance, R, which is given by Fresnel's law at the air/glass interfaces. Considering a PET substrate ($\varepsilon_r = 3$ and $\tan\delta = 0.003$), the optical reflectance is approximately 7.2%. In turn, the theoretical transparency, T_r, of the structures represented on Figure 1, can be calculated as:

$$T_r = (1-R)^2 \cdot \mathrm{OT} = 0.86 \cdot \mathrm{OT}. \tag{3}$$

Figure 2 displays the theoretical transparency, T_r, of a single layer of metalmesh and of stripes, as a function of spacing (s) and width (w). As expected, an increase of s leads to an increase of the transparency of both the structures. Conversely, an increase in w leads to a decrease in transparency. An increased level of transparency in the striped structure compared to the meshed structure for the same values of s and w parameters is observed. This is attributed to the larger open area in the striped structure, thereby resulting in improved transparency by $\frac{s+w}{s}$, as can be figured from equation 1 and 2.

If the thickness of a continuous metal layer, t, is higher than 1 μm, its sheet resistance $R_\square$, can be calculated by [8]:

$$R_\square = \frac{1}{\sigma t}. \tag{4}$$

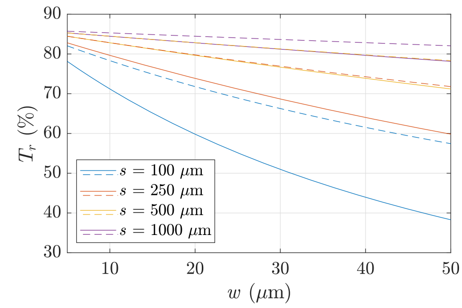

Figure 2. Theoretical transparency for mesh (solid lines) and stripe (dashed lines) structures as a function of mesh width (w) and mesh spacing (s).

The presence of apertures in metalmesh layers leads to an increase in the sheet resistance. The sheet resistance of a metalmesh can be expressed as follows:

$$R'_\square \approx \left(1 + \frac{s}{w}\right) R_\square. \tag{5}$$

The previous equations demonstrate that the structures depicted in Figure 1 face a significant challenge due to the inherent trade-off between their sheet resistance and optical transparency. An increase in T_r leads to an increase in $R'_\square$. Consequently, these results underscore the need to strike a balance between the conductivity ($R'_\square$), width, space, and thickness of the metal to optimise the antenna performance.

Figure 3 depicts the reflection and transmission amplitudes of the structures of Figure 1 under linear y-polarized wave incidence, obtained on CST Studio Suite. As can be seen, the striped structure of Figure 1 (b) presents a slightly better performance in comparison with the metalmesh of Figure 1 (a). This behaviour was already seen in [9] for electromagnetic interference shielding. This may be due to small leakage currents in the direction perpendicular to the polarization of the wave in the metalmesh structure.

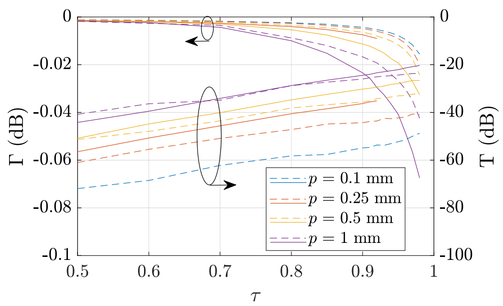

Figure 3. Reflection and transmission amplitude for mesh structure (solid lines) and stripe structure (dashed lines), under y-polarized wave incidence at 6.5 GHz ($p = s + w$ and $\tau = \frac{s}{s+w}$).

2.3 Design Procedure

The unit-cell, shown in Figure 4, has an area of 23 × 23 mm^2 ($\lambda_0/2 \times \lambda_0/2$ at 6.5 GHz, where λ_0 is the wavelength in free space). To allow optical transparency a 2 mm thick PET substrate was used. The radiating element consists of a silver ($\sigma = 6.3 \times 10^7$ S/m) metalmesh rectangular patch antenna, with a $L = 7.5$ mm and $W = 11$ mm, on top of the substrate and a silver stripe layer at the bottom. As the polarization of the unit cell is linear, along the y-direction, the current flow in the ground plane is mainly along that direction [5], so stripes are employed in the bottom layer to enhance transparency.

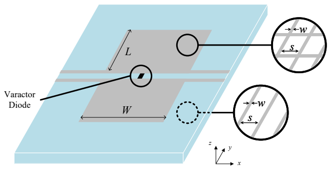

Figure 4. Geometry of the proposed RIS unit-cell.

This unit-cell employs concepts that were developed for frequency agile antennas. It operates by electronically modifying the resonant frequency and, in turn, the reflected phase of a patch using a varactor diode, that serially connects the two halves of the patch. The MGV-100-20 gallium arsenide (GaAs) varactor diode was chosen for the unit-cell design, and a gap of $g = 0.5$ mm was used for it. To understand how the linewidth (w) affects the radiation properties of this transparent antenna, keeping the optical transparency ($\tau = 0.95$), two cases were considered: $w = 25$ μm with $s = 0.475$ mm and $w = 12.5$ μm with $s = 0.2375$ mm. The theoretic sheet resistance is approximately 0.3 Ω/sq. It should be noted that the number of lines on the bottom layer and of squares of the patch were adjusted to maintain a constant optical transparency.

2.4 Simulation of the unit-cell

The simulation of the unit-cell was carried out using the Frequency Solver of CST Studio Suite, with unit-cell boundary conditions on the lateral faces of the unit-cell. The boundary conditions impose a Floquet port excitation under linear polarization and normal incidence. The incorporation of a varactor diode into the unit-cell on the simulator was achieved by using a lumped element with its corresponding equivalent circuit, an *RLC* series, with $R = 0.7$ Ω, $L = 0.4$ nH and $C = 0.12$ - 1.8 pF. The capacitor value was varied within this range, which correlated to the applied bias (the capacitance decreases as the controlling voltage increases). Figure 5 depicts the phase of the reflection coefficient obtained by simulation of a non-transparent version unit-cell for reference, as a function of the capacitance (the top and bottom layers were replaced with a continuos silver film). The four coding states indicated in Figure 5 (s_1, s_2, s_3, s_4), are separated by 90° between them, and correspond to capacitances of 0.12 pF, 0.215 pF, 0.27 pF and 0.52 pF.

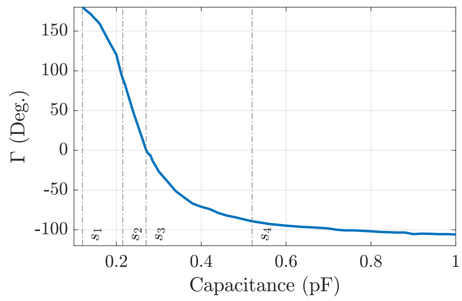

Figure 5. Reflection phase of the non-transparent unit-cell as a function of the capacitance of the varactor diode.

Figures 6 (a) and (b) depict the reflection coefficient's magnitude and phase, respectively, for the four states, obtained by simulation in the frequency band studied and for the three cases under study. The grey shadowed areas represent the operational frequency range of the RIS element, which spans from 6.23 to 6.8 GHz (maximum phase deviation of 45°, for the non-transparent version and for the $w = 0.125$ μm). As demonstrated in Figure 5, the adjacent phase states exhibit a phase difference of approximately 90° in the vicinity of 6.5 GHz.

For the transparent unit-cells, the reflection amplitudes exhibit levels greater than -3 dB, allowing for phase modulation with minimal loss. Theoretical OT of the top layer was calculated as approximately 96%, and 95% for the bottom layer (approximately 5% more than would be achieved with a metalmesh). Therefore, the estimated light transmittance, T_r, of the RIS element is about 79%, which is similar to the results obtained in [5]. Furthermore, this result represents a 30% improvement over the design presented in their earlier work [10].

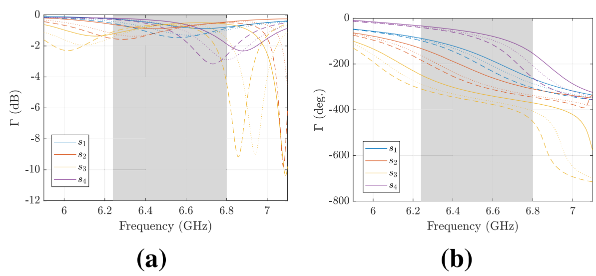

Figure 6. (a) Magnitude and (b) phase of the three unit-cells reflection coefficient for the four states (non-transparent in solid line, $w = 0.25$ μm in dashed line and $w = 0.125$ μm in doted line).

3 Metalmesh-based RIS

The presented 2-bit optically transparent unit-cells based on a metalmesh can be used to implement a linearly-polarized beam-steering RIS for diverse scan angles. The far-field pattern scattered by the RIS can be calculated by the superposition of the scattering wave from each cell as [11]:

$$f(\theta,\varphi) = \sum_{m=1}^{M}\sum_{n=1}^{N} |\Gamma_{mn}| e^{-j[\Phi_{mn} + kd \sin\theta (m\cos\varphi + n \sin\varphi)]}, \quad (6)$$

where $|\Gamma_{mn}|$ and Φ_{mn} are the magnitude and phase of the reflection coefficient of the unit cell located at position [m, n], k is the wavenumber in free space, d is the period of the RIS and θ and φ are the elevation and azimuth angles in a spherical coordinate system.

A simulation was conducted on CST Studio Suite to demonstrate the beam steering ability of the proposed optically transparent RIS using a 16×16 elements array, with $w = 0.125$ μm. As depicted in Figure 7, the simulation yielded far-field scattering patterns for four different steering angles, according to the phase profile imposed in the RIS, namely $\theta = 10°$, $20°$, $30°$, and $40°$. The theoretical results, obtained through equation 6, agree well, as expected.

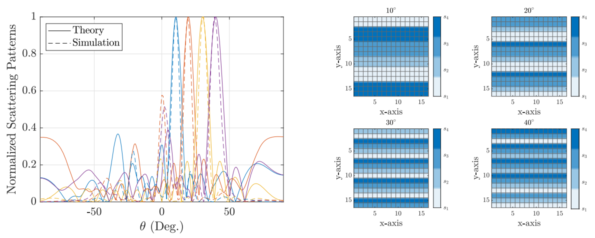

(a) **(b)**

Figure 7. (a) Normalized scattering patterns for different steering angles (b) The different phase distributions used.

4 Conclusion

A transparent unit-cell for reflective intelligent surfaces was proposed for Wi-Fi 6E applications. The unit-cell consists of an optically transparent PET substrate, a metalmesh patch with a varactor diode, and a stripe ground plane. The unit-cell can change the reflected phase over 290°, allowing for four different states of reflected phase and the implementation of a 2-bit RIS. The proposed unit-cell was used to design a transparent RIS consisting of 16×16 elements, which was illuminated by a plane-wave, and the full-wave simulation patterns were observed for 10°, 20°, 30° and 40°, consistent to theoretical predictions. The metalmesh-based RIS that has been proposed shows great potential for use in scenarios involving RIS-assisted wireless networks that require optical transparency (for example, in building windows or above solar panels, allowing light to pass through without affecting their efficiency).

5 Acknowledgements

This work is financed by National Funds through the FCT - Fundação para a Ciência e a Tecnologia, I.P. (Portuguese Foundation for Science and Technology) within the project TORIS, with reference 2022.09084.PTDC (DOI 10.54499/2022.09084.PTDC). This work was supported by FCT/MCTES under grant 2020.04948.BD.

References

[1] E. Reshef and C. Cordeiro, "Future directions for wi-fi 8 and beyond," *IEEE Communications Magazine*, vol. 60, no. 10, pp. 50–55, 2022.

[2] T. D. Nguyen, Y. Lee, and C. W. Jung, "Transparent and flexible patch antenna using mmf for conformal wifi-6e applications," *Journal of Electromagnetic Engineering and Science*, vol. 23, no. 4, pp. 310–317, 2023.

[3] W. A. Neamah, H. M. Al Sabbagh, and H. Al-Rizzo, "A compact two-element linearly and orthogonal circularly polarized mimo antenna system for 5g cellular and wlan/wi-fi 6e application," *IEEE Access*, 2023.

[4] R. B. Green, K. Ding, V. Avrutin, U. Ozgur, and E. Topsakal, "Optically transparent antenna arrays for the next generation of mobile networks," *IEEE Open Journal of Antennas and Propagation*, vol. 3, pp. 538–548, 2022.

[5] J. C. Liang, P. Zhang, Q. Cheng, and T. J. Cui, "Reconfigurable intelligent surface with high optical-transparency based on metalmesh," *Journal of Information and Intelligence*, vol. 1, no. 3, pp. 228–237, 2023.

[6] S. Hu, F. Rusek, and O. Edfors, "Beyond massive mimo: The potential of data transmission with large intelligent surfaces," *IEEE Transactions on Signal Processing*, vol. 66, no. 10, pp. 2746–2758, 2018.

[7] N. Ojaroudi Parchin, H. Jahanbakhsh Basherlou, Y. I. Al-Yasir, A. M. Abdulkhaleq, and R. A. Abd-Alhameed, "Reconfigurable antennas: Switching techniques—a survey," *Electronics*, vol. 9, no. 2, p. 336, 2020.

[8] J. Hautcoeur, X. Castel, F. Colombel, R. Benzerga, M. Himdi, G. Legeay, and E. Motta-Cruz, "Transparency and electrical properties of meshed metal films," *Thin Solid Films*, vol. 519, no. 11, pp. 3851–3858, 2011.

[9] P. Banerjee, Y. Bhattacharjee, and S. Bose, "Lightweight epoxy-based composites for emi shielding applications," *Journal of Electronic Materials*, vol. 49, pp. 1702–1720, 2020.

[10] J. C. Liang, Y. Gao, Z. W. Cheng, R. Z. Jiang, J. Y. Dai, L. Zhang, Q. Cheng, S. Jin, and T. J. Cui, "An optically transparent reconfigurable intelligent surface with low angular sensitivity," *Advanced Optical Materials*, p. 2202081, 2022.

[11] P. Nayeri, F. Yang, and A. Z. Elsherbeni, "Reflectarray antennas: theory, designs, and applications," 2018.